Journal of the European Ceramic Society 42 (2022) 5789–5800

Contents lists available at ScienceDirect

Journal of the European Ceramic Society

journal homepage: www.elsevier.com/locate/jeurceramsoc

Impact of sintering temperature on phase composition, microstructure, and porosification behavior of LTCC substrates

Ali Hajian [a,b,*], Anna Artemenko [c], Alexander Kromka [c], Sabine Schwarz [d], Michael Schneider [a], Kateřina Dragounová [c], Manikandan Adaikkan [b], Christopher Zellner [a], Ulrich Schmid [a]

[a] Institute of Sensor and Actuator Systems, TU Wien, 1040 Vienna, Austria
[b] VIA electronic GmbH, 07629 Hermsdorf, Germany
[c] Czech Academy of Sciences, Institute of Physics, Prague 16253, Czech Republic
[d] University Service Centre for Transmission Electron Microscopy, TU Wien, Wiedner Hauptstrasse 8-10, 1040 Vienna, Austria

ARTICLE INFO

Keywords:
LTCC
Sintering
Glass-ceramics
Porosification
Crystallization

ABSTRACT

Phase development and changes in crystalline composition of LTCC material during the sintering process were investigated using *in-situ* X-ray diffraction (XRD) measurements. CeramTape GC was chosen as the chemically simplest model system composed of alumina particles and glass for the investigations. The chemical characterization and microstructural analyses of the tapes sintered with some representative firing profiles were performed by techniques such as (scanning) transmission electron microscope, energy-dispersive X-ray spectroscopy, Raman spectroscopy, X-ray photoelectron spectroscopy, and XRD. Moreover, the porosification behavior of LTCC substrates fired at different peak temperatures was studied. These investigations are important for the subsequent wet chemical etching, representing an approach which allows to reduce locally the permittivity of LTCC tapes. Treatment with a KOH solution shows non-selective etching behavior for all substrates. In addition, highly porous silica structures corresponding to Ca and Al depletion from the anorthite phase were observed in all samples after etching treatment.

1. Introduction

LTCC (low temperature co-fired ceramics) is an outstanding technology platform that has attracted considerable attention for microelectronics and sensors. LTCC technology is largely used for different applications such as (bio)medical, sensors, and electrochemical devices [1–4]. However, its main demand is in automotive and telecommunication areas [5–9]. LTCC is the technology of choice when targeting the realization of highly integrated wiring or packaging solutions for systems operated at high frequencies typically ranging up to the microwave region. This technology was developed to improve the properties of the existing high-temperature cofired ceramics (HTCCs) multilayer circuits. Further outstanding features of the LTCC such as superior thermal conductivity compared with organic materials, and a coefficient of thermal expansion (CTE) close to silicon, make it more suitable compared to organic-based multilayer substrate [6,10]. Silicon-on-Ceramic (SiCer) substrates, which can be fabricated and processed using LTCC and MEMS technologies, ensure passive electronic functionality owing to the LTCC part and thin-film processing for MEMS components owing to the Si component [11].

From the material point of view, LTCC material systems are based on unfired (green) ceramic tapes which are produced through a tape casting process. The green tape is typically a composite of organic material, glass frit, and ceramic filler. The filler material choice depends on the dielectric requirements of the microelectronic device. The most commonly used filler materials are alumina, fused silica, mullite, barium titanate, and cordierite ([12–15]. The addition of glass frits with low glass transition temperature is necessary as it lowers the sintering temperature of the ceramics below the melting point of co-fired electrode materials because otherwise none of these filler materials can be densified in the pure form at temperatures below 900 °C. Through a firing process, first organic additives including binders and plasticizers are driven off during the debinding phase, followed by sintering. Sintering temperatures lower than 900 °C allow the use of high electrical conductivity noble metal pastes such as Ag, Au, AuPt, and AgPd for co-firing, which improves the performance of multilayer devices [13].

The low processing temperature of LTCCs can be achieved by using three main types of materials: a glass-ceramic composite, a crystallizing

* Corresponding author at: Institute of Sensor and Actuator Systems, TU Wien, 1040 Vienna, Austria.
E-mail address: ali.hajian@tuwien.ac.at (A. Hajian).

https://doi.org/10.1016/j.jeurceramsoc.2022.05.049
Received 8 January 2022; Received in revised form 16 May 2022; Accepted 22 May 2022
Available online 26 May 2022

glass system, and a non-glass system (the green ceramic does not contain an amorphous phase). Of these, the "Glass Ceramic Composites (GCC)" system is the most commonly used tape system and is also the focus of the present study. Other types of LTCC materials concerning their composition, material properties and sintering mechanisms have been reported in the literature [16,17].

These GCC systems are usually designed in such a way that partial crystallization of the glass occurs during the firing process, minimizing the amount of glass phase in the composite and affecting the mechanical and electrical properties of the glass-ceramic material. Depending on the requirements of the intended application, different composite models were fabricated and investigated. A commonly used ceramic filler is Al_2O_3. This filler is capable of reacting with the glass phase at high temperatures, resulting in a hermetic composite substrate material. During the firing process, the inorganic components with respect to their particular composition are densified. The resulting *as-fired* LTCC material is basically composed of a glass matrix in which crystalline particles with a typical micrometer-range diameter are embedded as filler material [18–20].

The most critical part of the LTCC technology is the sintering behavior of the glass-ceramic and microstructure development during cofiring [18]. To convert the LTCC green tape into a solid, dense material, it needs to undergo a sintering process. Three common types of sintering processes are: (a) *viscous flow,* (b) *liquid phase*, where a liquid is formed during the sintering process and solid grains are soluble in the liquid; and (c) *solid-state*, where the sintering occurs between touching particles through diffusion [13,21,22]. In the case of LTCC tapes, due to the glass component, the process is most significantly of viscous flow type. A detailed overview of the reactions of alumina as the most common filler material with glass phases of different compositions was given by Müller et al. [23]. They investigated the dissolution of alumina, the sintering behavior, and the crystallization of glass-ceramic model systems. The glass components were in the liquid phase at the sintering temperature, while (alumina) grains remained in the solid state. Due to compatible surface free energies and capillary forces, the alumina grains got wetted. With a decrease in temperature, the crystallization of the glass started, and solid material was formed. Since the glass component of the LTCC became viscous during the sintering process, part of the alumina could dissolve into the glass phase. The result of that was the formation of anorthite, $CaAl_2Si_2O_8$, phases or similar framework silicates (*e.g.* labradorite, $(Ca,Na)Al(Si,Al)_3O_8$, or celsian, $Ba[Al_2Si_2O_8]$). The influence of the firing temperature and time on the phase composition and microstructure of DuPont 951® tape was investigated by Makarovič et al. [16]. They detected an increase in the anorthite phase when the firing temperature or the firing time was increased until reaching a plateau at *ca* 22 wt%, while at the same time, a decrease in glass content was observed. The observed changes in phase composition and microstructure were found to affect the flexural strength and CTE of LTCC test specimens.

Investigation of the sintering behavior of the ceramic filled glass composites is of great importance as it substantially affects the physical and chemical properties of the resulting substrate. Even though several publications focus on the LTCC technology, only a few of them have discussed the sintering behavior and microstructural development of LTCC materials [13,16,18,24,25]. Therefore, in this paper, morphology, microstructural development, and chemical surface composition investigations are performed as a function of peak firing temperature and correlated among each other. These findings will be useful for tailoring new LTCC systems in terms of the physicochemical properties, as well as for understanding the densification mechanism of the tapes for *e.g.* a better shrinkage control.

While LTCC materials feature attractive thermal, mechanical and dielectric properties that make them highly suitable for various applications such as wireless communications or automotive radar systems, their use in high-frequency devices is limited. Patch antenna integration and accurate design of micromechanical structures operating at high frequencies require separate regions with tailored permittivities for optimized radiation performance. Whereas regions with low permittivity improve both bandwidth and efficiency of active components, those with high permittivity enable the design of compact power supply circuits.

To fulfill this objective, a practical strategy is to replace some of the high-k LTCC components with very low permittivity air ($\varepsilon_r = 1$) using a wet chemical etching process as first reported in [26]. Further studies on the wet chemical etching of various LTCC systems under different conditions provided important information on the porosity mechanism [27–29]. It was found that etching under acidic conditions is more selective and the feldspar component of the tape is dissolved more rapidly, which can lead to high porosity. On the other hand, etching under alkaline conditions is less selective and the glass portion of the LTCC is also attacked. The latter has proven useful for modifying the surface area and substrate thickness.

In the present work, the porosification behavior of LTCC substrates fired at different peak temperatures was studied. These investigations are important for further improving the wet chemical etching process. Moreover, this work offers a more accurate approach to optimize the firing profile of the specimens compared to traditional densification and shrinkage measurements.

2. Experimental procedure

Commercially available LTCC tape, CeramTape GC (Ceramtec, Marktredwitz, Germany) was used as a model system for investigating the impact of sintering temperature on the crystallization behavior as well as microstructure. CeramTape GC, a well-investigated LTCC system, is composed of a calcium aluminosilicate glass filled with 30–45 vol % alumina particles with a particle size of approximately 1.0–1.5 μm [30,31].

The first step of sample preparation involves the cutting of the unfired tapes into the desired shape using a diode-pumped Nd:YAG-Laser (ROFIN Sinar, Germany) equipped with an acoustic optical switch and an objective lens with a focal length of 160 mm, as well as a computer-controlled galvanometric beam deflection system (operating power: 12 W at TEM00-mode). Parameters used for the cutting were optimized based on Smetana et al. who have investigated the cutting behavior of different LTCCs [32].

A six-zone belt furnace (BTU SYSTEMS) was used for firing LTCC specimens. Temperature of each zone, airflow, and the belt speed were programmed using an industrial controller (PMA, KS 40-1). The belt furnace offers the advantage that it can be operated continuously at very short cycle times. Due to the inherent temperature gradient along the transport direction the belt furnace is suitable for rather thin and small substrates as in the present study. To prevent specimen contamination within the furnace environment, they were enclosed between two CeramTec A-Tapes on a base alumina setter, and no pressure and lamination were applied. A-tape serves as a sacrificial material and after firing converts to a very brittle sheet which is easily removed from the fired LTCC substrates.

GC LTCC green tapes were subjected to different firing profiles with varied peak temperature for *ca* 70 min total sintering cycle. The firing process was conducted at nominal peak temperatures between 800 and 950 °C and the impact of peak firing temperature on the morphology and composition of the LTCC substrates were studied. It should be mentioned that the actual temperature of the furnace for all firing profiles was measured by using a thermocouple type K (NiCr/Ni) and a deviation of about −10 °C from the nominal temperatures was detected. Therefore, to avoid misinterpretation the measured values are given in this study. The fired CeramTape GC LTCC samples were labeled as GC*z*, where *z* is the actual peak temperature used in the firing process. For example, GC890 refers to the GC LTCC fired at the peak temperature of 890 °C (*i.e.* nominal peak temperature of 900 °C).

For the morphological and microstructural analyses, a Hitachi

SU8030 field emission scanning electron microscope applying the secondary electron (SE) detection mode was used. No metal coating was applied on the surface of specimens before characterization and an operating voltage of 2 kV in charge suppression scanning mode was used. In addition, detailed analyses of crystallization and micro-/nanostructure were performed using a FEI Tecnai F20 (scanning) transmission electron microscope ((S)TEM) employing the high angle annular dark-field (HAADF) detector. This technique is very sensitive to the chemical composition as the HAADF detector collects Rutherford scattered electrons. The amount of Rutherford scattering depends on the square of the mean atomic number and thus on the chemical composition. Crystalline and amorphous phases were also identified based on selected area electron diffraction (SAED) patterns. Local chemical analyses were performed on the specimens using energy-dispersive X-ray spectroscopy (EDX). Electron energy loss spectroscopy (EELS) was carried out using a Gatan GIF Tridiem ER energy filter which is placed in the irradiation beam. The peaks in the EDX and EELS spectra were used for determination of the compositional ratio of the elements presented in LTCC samples. The collective application of these complementary techniques allowed the determination of most of the chemical components, their distribution as well as their state of crystallinity. For these investigations, LTCC specimens with a thickness in the range of few nanometers were prepared by using "lift-out" technique in a dual-beam focused ion beam (DBFIB) FEI Quanta 200 3D system.

XRD investigations were performed with a PANalytical X'PertPro MPD diffractometer providing a filtered X-ray beam from a Cu anode. A Soller collimator in the primary and secondary beam path provided a 0.04 rad divergence of the beam. The scans were taken from 5° to 90° with a step size of 0.02° in a continuous mode utilizing an X'Celerator detector with an opening of 2.1°. To detect possible X-ray amorphous fractions in the diffraction diagram, each point was measured with a scan speed of up to 4 s/step. The phase analysis based on the X-ray diffraction diagrams was performed using the High Score Plus software. Moreover, for the *in-situ* XRD monitoring of the crystallization behavior, LTCC green tapes were temperature loaded in time sequences with a representative heating profile shown in Fig. 1. This temperature profile provides information regarding the phase development at different peak temperatures up to 1000 °C. After increasing the temperature at each step, the temprature was kept constant for 24 min while recording the corresponding diffractogram. All measurements were performed in air.

Raman spectra of the films were measured at room temperature by a Renishaw In Via Reflex Raman spectrometer using a CCD camera and an excitation wavelength of 442 nm. Calibration of the spectrometer was performed with respect to the 520.7 cm^{-1} line of single-crystal silicon.

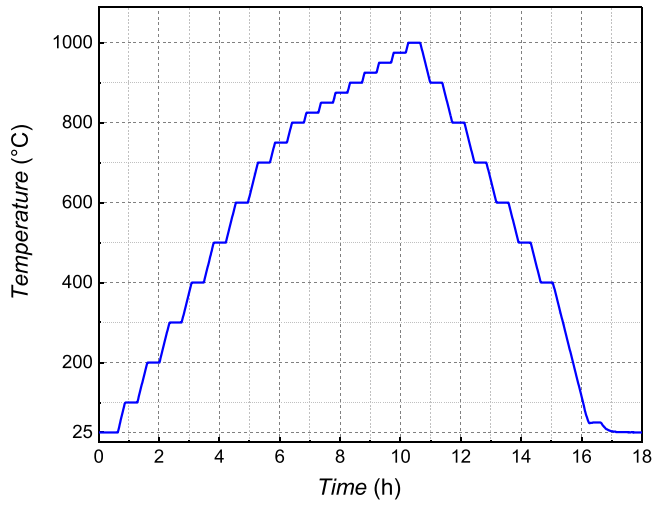

Fig. 1. The heating profile applied during *in-situ* sintering of GC LTCC while performing XRD measurements.

The impact of inhomogeneity of LTCC samples was minimized by taking measurements at different sample positions.

Furthermore, X-ray photoelectron spectroscopy (XPS) analysis was performed with an ultra-high vacuum AXISSupra photoelectron spectrometer (Kratos Analytical Ltd., UK) equipped with a hemispherical analyzer and monochromatic Al Kα source (1486.6 eV, analyzed area – 0.7 × 0.3 mm^2). The spectra were collected at the take-off angle 90°. The survey XPS spectra were recorded with a pass energy of 80 eV, whereas the high-resolution spectrum scans with a pass energy of 20 eV. The Kratos charge neutralizer system was used to compensate charging effects on the sample surface. The obtained XPS spectra were calibrated on the C 1 s peak maximum at 285 eV [33]. The CasaXPS processing software with Shirley baseline and Gaussian line shapes of variable widths for peak fitting was used for spectra processing. XPS peak positions were determined with an accuracy of ± 0.2 eV.

Thermal characterization of the LTCC tape was performed by thermogravimetric-differential thermal analysis (TG-DTA) and thermogravimetric analysis-differential scanning calorimetry (TG-DSC) using Themys TG-DTA 1600 and TG-DSC Netzsch STA 409PC/PG, respectively. The thermal analyses were conducted in air atmosphere with a heating rate of 3 ∘C/min. The DSC reveals chemical reactions and in combination with TG the temperature of complete binder burnout can be determined. The TG curve illustrates the changes in weight of the specimen with temperature, whereas the derivative of the TG curve (dTG) shows the weight loss rate of the specimen at a given temperature.

Selected samples were subjected to a wet chemical porosification process with an aqueous potassium hydroxide (KOH) solution. The etching solutions with the concentration of 3 mol L^{-1} were freshly prepared by dissolving the calculated amount of KOH pellets (≥99.97 % from Sigma-Aldrich) in deionized water. During the etching process, specimens were fixed with a polytetrafluoroethylene (PTFE) holder, and the solution was continuously stirred at 120 rpm to homogenize the exchange of the reactants and products. After the etching process, the LTCC samples were immediately rinsed thoroughly with deionized water as well as isopropanol and then dried in atmospheric air.

3. Results and discussions

3.1. Crystalline phase development

Crystallization behavior of the LTCC was examined by the *in-situ* XRD measurements from room temperature up to 1000 °C, and the corresponding diffractograms are shown in Fig. 2. At room temperature, which corresponds to the "green state", the corundum filler was the only detected crystalline phase. By rising temperature up to 825 °C, no crystallographic changes were observed (see Fig. 2a). At a temperature of 850 °C a new peak appears at around 31°, which can be attributed to the formation of a calcium silicate (wollastonite) phase [23,24]. Further increasing of temperature above 875 °C, new peaks appear, corresponding to crystallization of the anorthite phase from the glass phase matrix. Unlike anorthite, wollastonite crystals do not grow preferentially in the vicinity of corundum grains, but at the interface between glass pores [23]. A further temperature increase up to 925 °C leads to the formation of an additional anorthite phase while simultaneously the wollastonite fraction decreases. Beyond 925 °C, no perceptible change in the diffractograms can be observed, except for the slight increase in the intensity of the newly formed anorthite peaks together with the decrease in the intensity of the corundum peaks. Furthermore, the wollastonite almost disappears above 950 °C. Therefore, the increase of anorthite content between 850 and 900 °C is mainly due to the dissolution of dispersed alumina particles, while at temperatures above 925 ℃, the increase in anorthite content is due to the dissolution of dispersed alumina particles and wollastonite phase (see Fig. 2b). The simultaneous formation of anorthite and dissolution of alumina was already confirmed in a similar LTCC system by Müller et al. [23]. Based on this study, wollastonite crystals grow into the interior of glass (G_0), in

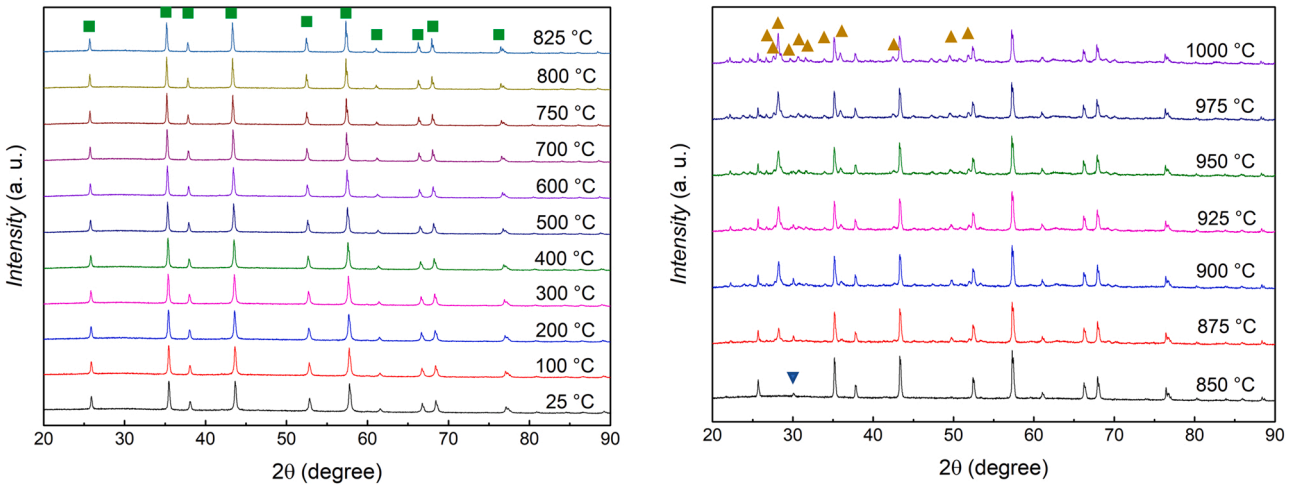

Fig. 2. In situ X-ray diffractograms of a GC LTCC subjected to different temperatures between 25 and 1000 °C (FX1: corundum, FX2: anorthite, FX3: wollastonite). The intensity levels are shifted for comparison reasons.

the first step (see reaction 1). Next, anorthite crystallization occurs as a result of two solid phase-boundary reactions: (*i*) dissolution of corundum and reduction of the amount of residual glass phase (see reaction 2):, and (*ii*) dissolution of corundum and wollastonite, without a further substantial reduction of the residual glass mass fraction (reaction 3). These two steps can be illustrated by the following reactions:

$$G_0 \rightarrow Wollastonite + G_1 \quad (1)$$

$$Corundum + G_1 \rightarrow Anorthite + G_2 \quad (2)$$

$$Corundum + Wollastonite + G_2 \rightarrow Anorthite + G_3 \quad (3)$$

where G_1 and G_2 refer to the residual glasses after wollastonite and anorthite crystallization, respectively, and G_3 shows the resulting residual glass upon the second stage of anorthite crystallization.

Based on the obtained results and discussed mechanisms, temperatures between 875 and 925 °C are recommended for the firing of GC LTCC. This is also in good agreement with the values given in literature [34]. The relatively high maximum firing temperature for GC LTCC, which is for example about 40 °C higher than for 951 LTCC from Dupont, can be explained by the low amount of viscosity lowering glass modifier oxides in GC LTCC [35].

3.2. Morphological investigations

Fig. 3 represent SEM morphologies of the LTCC in the green state and after firing at different peak temperatures. The results confirm that for GC790 no effective sintering occurs, and the surface morphology is very similar to that of the unfired tape. When the firing peak temperature is increased to 840 °C, the LTCC densifies due to the softening and diffusion of the glassy phase, and the discrete grains interconnect. Nonetheless, many large open pores and gaps between individual grains can still be observed on the surface. The densification starts with softening of the glass phase and continues with its viscous flow, what means that the sintering kinetics is predominantly controlled by the viscosity of the glass phase. In general, however, the densification mechanisms during the sintering process of LTCC are very complex and have been the subject of several studies [13,24,36].

The LTCC densification results are also in a good agreement with the bulk density values which were obtained by employing Archimedes

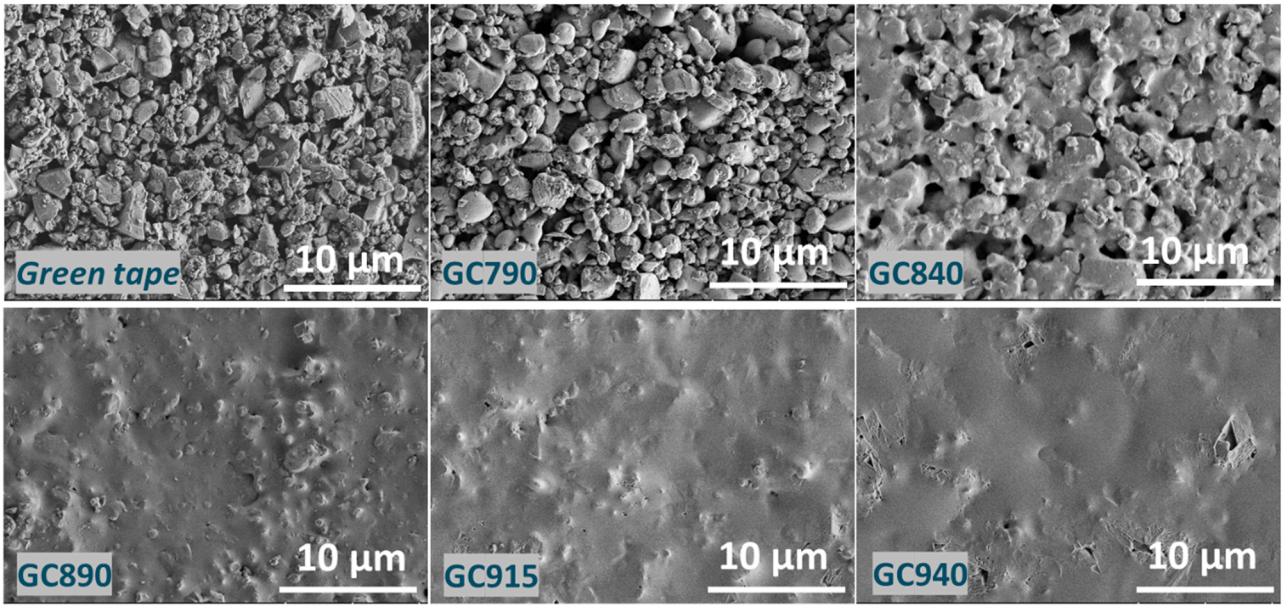

Fig. 3. SEM micrographs of the GC LTCC green tapes, as well as substrates sintered at different peak temperatures.

method (see Table 1).

In order to better visualize the grains after firing process, in addition to the secondary electrons used in Fig. 3, back scattered electrons were recorded during SEM imaging of the *"as-fired"* samples (see Fig. 4). Similar to the Fig. 3, for the samples sintered at and above 890 °C the interconnectivity of individual grains due to the glass diffusion can be observed.

By increasing the firing peak temperature to 890 °C, sintering becomes more effective, and a densified composite of glass matrix and ceramic filler is produced. However, due to the grains protruding from the surface, a rough topography with sharp edges results. When the firing peak temperature is further increased to 915 °C and then to 940 °C, the LTCC sample densifies more and its surface becomes much smoother, what is advantageous for subsequent metallization. The corresponding X-ray diffractograms for the samples fired at different peak temperatures in the belt furnace are depicted in Fig. 5. From these diffractograms, it appears that a sintering temperature of 840 °C is not high enough for the formation of the anorthite phase, and only a very small peak at around 31° is detectable, which is attributed to wollastonite crystallization. On the other hand, for the GC890 and above, the glass crystallizes partially to the anorthite phase. When the firing temperature is further increased to 915 °C, the intensity of the anorthite peaks increases, confirming the growth of anorthite crystals. However, the intensities of the peaks associated with the corundum grains remain almost unchanged, indicating that the dissolution of these grains has not yet started at these firing temperatures or is too minor to be detected. These results are in very good agreement with the high-temperature XRD results (*in-situ* temperature loading for an LTCC substrate) as shown in Fig. 2.

The samples were also subjected to TEM analyses, and the results shown in Fig. 6 give an overview of a green sheet analysed in dark field and bright field mode, respectively. The sample in the green state consists mainly of corundum grains and glass. The sample appears to be covered by a transparent and adhesive material, which is attributed to the organic components (binders, plasticizers, *etc.*) of the green sheet.

EDX analysis shows that the sample in the indicated area at the dark field image is mainly composed of Al, Si, O, Ca, and B. Three representative images were taken for SAED analysis, showing an amorphous glass phase and crystalline corundum grains in both areas 1 and 2. The boron-rich area (area 3) is also crystalline. No clear reason was identified for this finding as boron trioxide usually appears in the amorphous phase and also no crystalline phase other than corundum was found in the XRD pattern for the green tape (see Fig. 5). After annealing, however, boron trioxide can appear in crystalline form. Thus, this very small area which is found here could be attributed to the boron trioxide dissolved in the glass during the glass manufacturing process.

As mentioned above, increasing the peak temperature causes the LTCC substrates to densify to a higher degree, leading in addition to a smoother surface. This is caused by the diffusion of the glass to the LTCC surface, which results in filling the surface-near pores and also covering the protruding grains. This is an important request for a very smooth surface (*e.g.* for thin-film compatible LTCC) and also when porosification of the LTCC is targeted, as it is expected that the penetration of the etching solution into a glass-covered surface be different from that of a standard LTCC.

Table 1
Bulk density values for the substrates fired at different peak temperatures.

Sample	Bulk density (g cm^{-3})
GC790	2.37
GC840	2.76
GC890	2.84
GC915	2.88
GC940	3.10

3.3. Spectroscopic investigations

For crystallographic phase analysis, Raman measurements were performed revealing significant changes in the vibration modes for the fired samples (GC 790–940) compared to green sample (GC green tape), especially in the region of Raman shifts higher than 800 cm^{-1} (see Fig. 7) due to the presence of corundum in the glass-ceramic mixture. Peak assignment was performed using the RRUFF database, however, the interpretation of some individual peaks (like CaO (B_2O_3)) was complicated and all peaks could not be indexed (see Fig. 8). For the green tape, the spectrum is even more complicated due to the presence of both organic binder and plasticizer. However, during the firing process, these materials are completely burned out and the remaining peaks can be attributed to the inorganic constituents of the GC LTCC, which are produced from the firing of calcium aluminosilicate and the corundum filler. This also explains the significant difference in the Raman spectrum of the green tape compared to GC790, while almost no difference was found in the XRD diffractograms of the green tape with those sintered at temperatures up to 825 °C.

Raman spectra for the fired samples showed that the transformation of the overall vibrational structure starts at about 890 °C, thus indicating the onset of sintering which is in accordance with SEM and XRD investigations. For the GC890 sample, the presence of anorthite is more pronounced in the spectrum, while the corundum-related vibrational peaks dominate in the GC790 and GC840 spectra. By increasing the firing temperature especially for the GC940, the intensity of some corundum peaks decreases which is in good agreement with XRD analyses. Considering the temperature range, in which the specimens were prepared, the theta or gamma phase of alumina are expected, but they are not observed or are close to the detection limit. Nevertheless, these phases are metastable and their presence should be detectable in the Raman spectra for sintering temperatures below 890 °C [37,38]. Anorthite has also several phases (polymorphism), as reported in [39], but Raman spectra of particular phases do not differ significantly.

The chemical composition of the surface of the samples was analysed by XPS. Table 2, summarizes the relative atomic concentrations of the chemical elements detected on the samples. The significant decrease in the carbon concentration on the surface of the fired samples indicates the cleaning from hydrocarbon species due to the burnout of the organic components of the LTCC. Thus, for GC790 due to reduction in C content, the relative atomic concentration of all other elements increases significantly.

The increase of the calcium and boron signal in the case of fired samples in contrast to green tape was detected by XPS. The obtained XPS data from the surface of the samples correlate with observations of CaO (B_2O_3) peaks in bulk Raman spectra (see Fig. 8) indicating an enhanced diffusion of CaO (B_2O_3) glass to the top layer of the sample surface. Moreover, XPS analysis revealed a significant increase in the silicon content by the firing process (from 2.8 at% for the green tape to 13.1 at % for the GC790). By further increasing the firing temperature from 790 °C to 940 °C, the silicon content constantly increases up to 19.4 at %. In contrast to Si, the Al content decreases from 11.5 at% for the GC790 to 4.2 at% for both GC915 and GC940. These results hint towards the diffusion of the glass phase to the surface of LTCC and covering the alumina grains during firing and the densification phase. This is also in agreement with the morphological structure revealed by the SEM micrographs of GC LTCC substrates fired at different peak temperatures (see Fig. 3). For the GC890 in which anorthite growth occurs, the Ca count is maximum (5.4 at%) and decreases with increasing firing temperature to 4 at% for GC940. This behavior can be attributed to the formation of the anorthite phase in GC890 and as a consequence of the glass diffusion to the surface, this phase together with the enveloped alumina grains are covered.

Analysis of the high resolution XPS spectra of the fired samples showed a shift of about 0.5 eV in the peak maxima of the chemical elements to the region of higher binding energy compared to the green

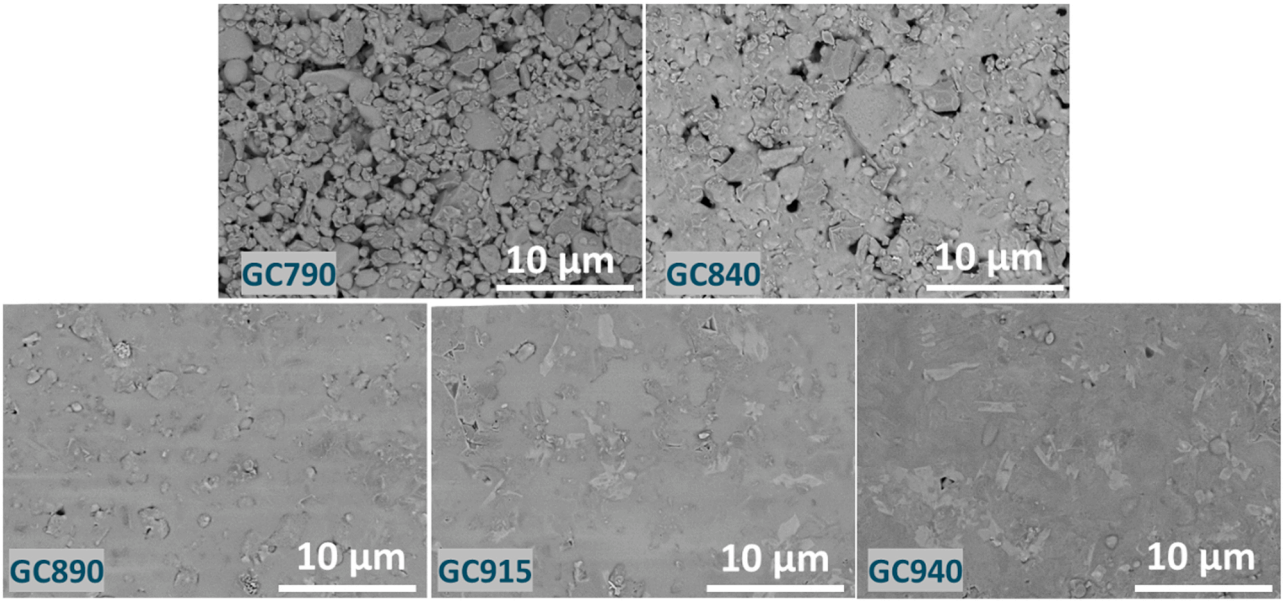

Fig. 4. BSE SEM micrographs of the GC LTCC sintered at different peak temperatures.

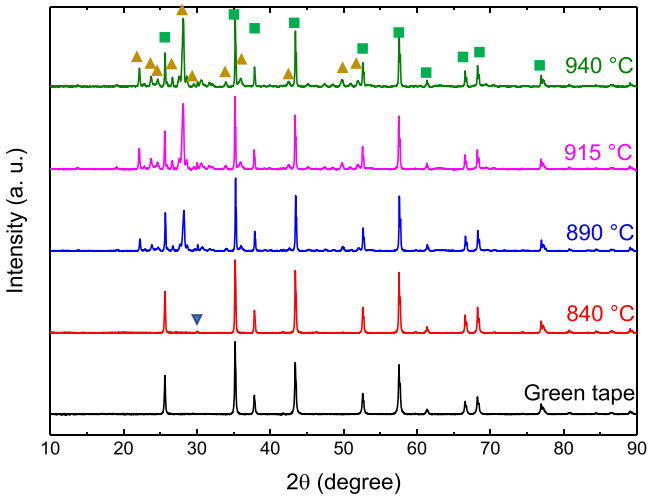

Fig. 5. X-ray diffractograms of GC LTCC green tapes fired at different peak temperatures (■: corundum, ▲: anorthite, ▼: wollastonite). The intensity levels are shifted for comparison reasons.

tape. The high resolution Al 2p peaks were deconvoluted into 3 peaks: α-Al_2O_3 (74.0 eV), transition-Al_2O_3 (75.0 eV) and Al-OH (76.0 eV). As the literature reports that the Al 2p spectra of successive transition aluminas (γ, δ and θ) cannot be distinguished by their chemical shift, it was proposed to introduce in the deconvolution process a transition alumina component with the fitting peak (transition-Al_2O_3) at a binding energy value of 75.0 eV [33].

Table 3 shows the chemical bond concentrations calculated from the deconvoluted Al 2p peaks. As the sintered LTCC samples contain both corundum (Al_2O_3) and anorthite ($CaAl_2Si_2O_8$) in their composition, the fluctuation of the aluminium bond concentrations could be explained either by surface reconfiguration caused by firing (anorthite replaced the corundum) or by the phase transition of corundum (as mentioned above in the Raman studies).

Fig. 9 shows the comparison of Al 2p peaks shapes of fired LTCC samples with the green tape deconvoluted Al 2p peak. At 840 and 940 °C, a slight shift of Al 2p to the higher binding energy region of about 0.2 eV was observed.

The high resolution Si 2p peaks were fitted with 3 peaks: SiC (100.6 eV), SiO_2/Si present in Al_2O_3, B_2O_3 and CaO (102.4 eV), SiO_2 (103.5 eV) [40,41]. The concentrations of chemical bonds are listed in Table 4. The significant increase of SiO_2 bond concentration from 25 % to 64.5 % correlates well with the increase of atomic concentrations of silicon and oxygen components on the surface of the fired samples. Fig. 10 shows the comparison of peak shapes of the sintered samples with the deconvoluted Si 2p peak of the green tape. As can be seen, the maximum of Si 2p peaks of the fired samples was shifted to the region of higher binding energy (from 102.6 to 103.1 eV).

Deconvolution of the high resolution O 1 s peak was performed in accordance with [33,42–45] into 3 peaks: O bulk (530.7 eV) [42], Al-OH/CaCO (532.1 eV) [42,43], B_2O_3/SiO_2/H_2O (533 eV) [42,44,45]. Table 5 presents the chemical bond concertation calculated from the deconvoluted O 1 s peaks. The significant decrease in B_2O_3/SiO_2/H_2O component concentration from 41 % to 14 % revealed the desorption of the H_2O molecules from the fired samples. However, increasing the temperature up to 940 °C most likely led to the increase in B_2O_3/SiO_2 bonds (from 14 % to 31 %) which correspond to the presence of CaO (B_2O_3) and anorthite on the sample surface. The changes in the O bulk concertation can be explained by the possible diffusion of the glass to the top surface of the fired samples.

Fig. 11 shows the comparison of O 1s peaks shapes of fired samples with the green tape deconvoluted O 1s peak. As can be seen, the firing caused significant changes of the O 1s peak shape (B_2O_3/SiO_2/H_2O bond at 533 eV decreased) and shifted the maximum of O 1s peaks of the fired samples to the higher binding energy region.

In addition, the analysis of the high resolution Ca 2p and B 1 s peaks was performed. According to [43] the Ca 2p peak has clearly spaced spin-orbit components: Ca $2p_{3/2}$ and Ca $2p_{1/2}$ split is about 3.5 eV. In the case of green tape and fired samples, the Ca 2p had also a double-split shape with a split distance of about 3.5 eV (Ca 2p spectra are not shown here).

As for the B 1 s peaks, for all samples, the position of B 1 s peak at about 192.4 ± 0.2 eV was attributed to B_2O_3 [46]. According to [47], the B 1 s peak at 192.4 eV corresponds to B^{+3} homogenously surrounded by oxygen tetrahedral. Moreover, elemental boron at 188 eV was not observed in any of the measured B 1 s peaks. The obtained B 1 s spectra (not shown here) are symmetric and could be fitted by a single chemical environment centered at 193.5 eV, which is attributed to B_2O_3 [48].

Moreover, EDX analysis was performed for the samples sintered at

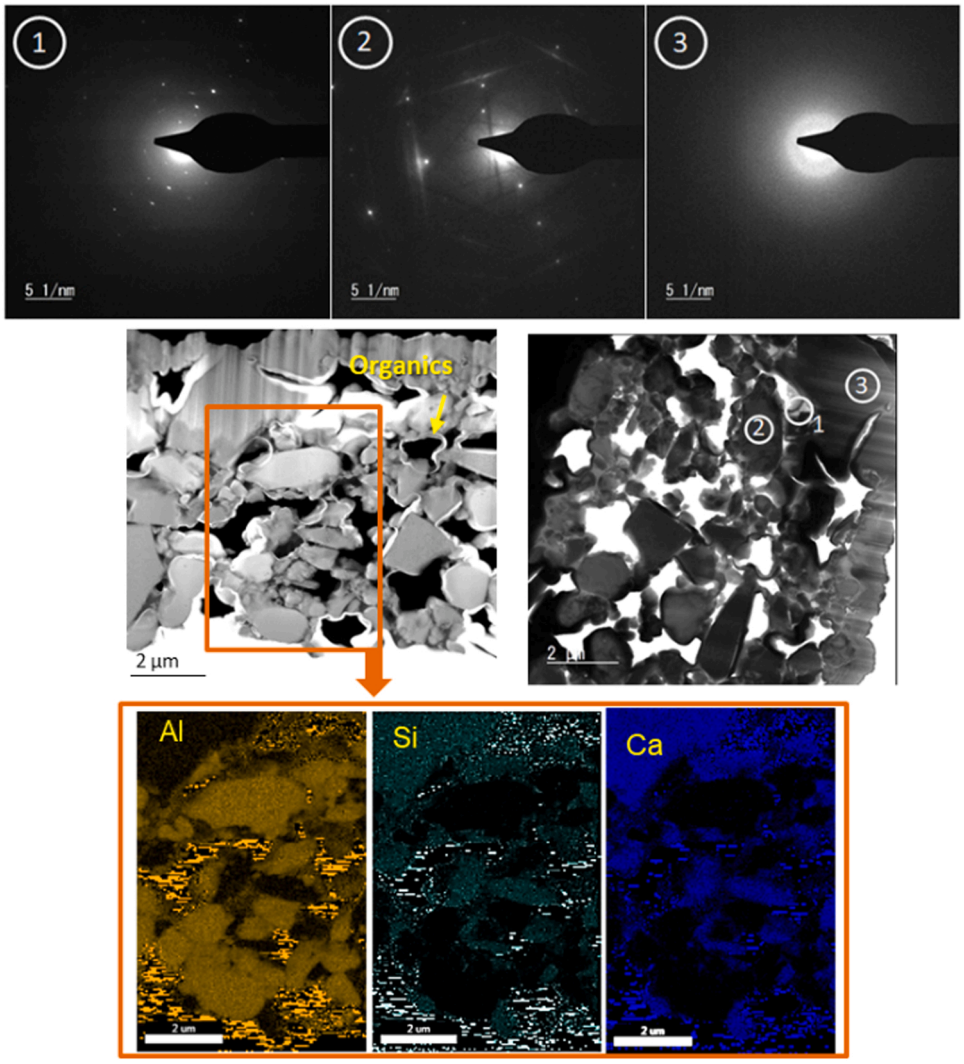

Fig. 6. TEM images of the GC LTCC green tape in the dark field (middle left), and bright field (middle right) mode. The bright-field image is clockwise rotated for 90 °. EDX mapping results for the indicated area (O is excluded) is shown in the bottom raw while SAED analyses of three locations labeled in the bright field image is shown in the top raw.

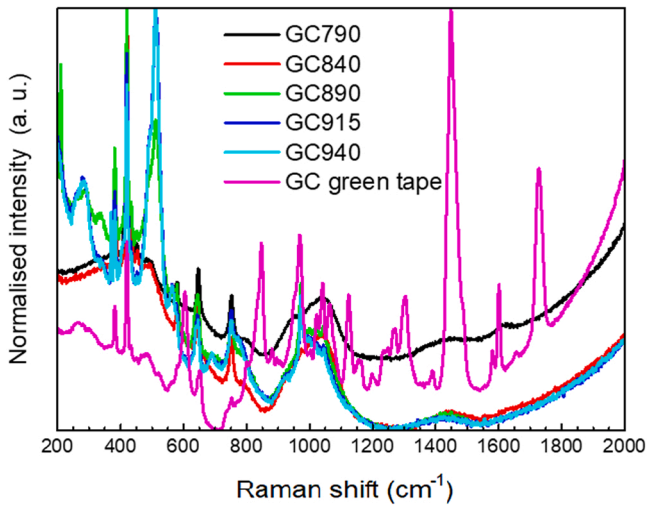

Fig. 7.. Normalized Raman scattering spectra for GC green tapes fired at different peak temperatures.

different peak temperatures, and the results are shown in Table 6. Although EDS is much less surface sensitive compared to XPS and is not suitable for quantitative analysis of light elements, the results obtained, especially for Al and Si, show good agreement with the XPS results. By increasing the firing temperature from 790 °C to 940 °C, the Si content increases continously from 10.3 to 13.3 at%. In contrast to Si, the Al content decreases from 18.9 at% for the GC790 to 13.9 at% for GC940. These results confirm the diffusion of the glass phase to the surface of LTCC while covering the alumina grains during firing and resulting in the densification phase.

Furthermore, TG-DTA and TG-DSC analyses were performed with the green tape. The results are presented in Fig. 12.

Thermal analysis of the CeramTape GC green tape shows a mass loss starting at *ca* 100 °C due to the evaporation of moisture and solvents. As can be seen in Fig. 12, organic components of the LTCC tape burnouts in two stages yielding a total weight loss of about 16.9 %. Burnout of the LTCC organic vehicle proceeds in an exothermic decomposition process, confirmed by the DSC curve, in the temperature ranges from 150 °C to 275 °C and from 275 °C to 375 °C with two separated peaks at the DTG curve. Weight of the LTCC tape remains constant for temperature above *ca.* 450 °C. The peaks at temperatures lower than 450 °C are attributed to organic additive burnout. A pronounced crystallization peak was observed with the onset point of crystallization at 875 °C. All obtained

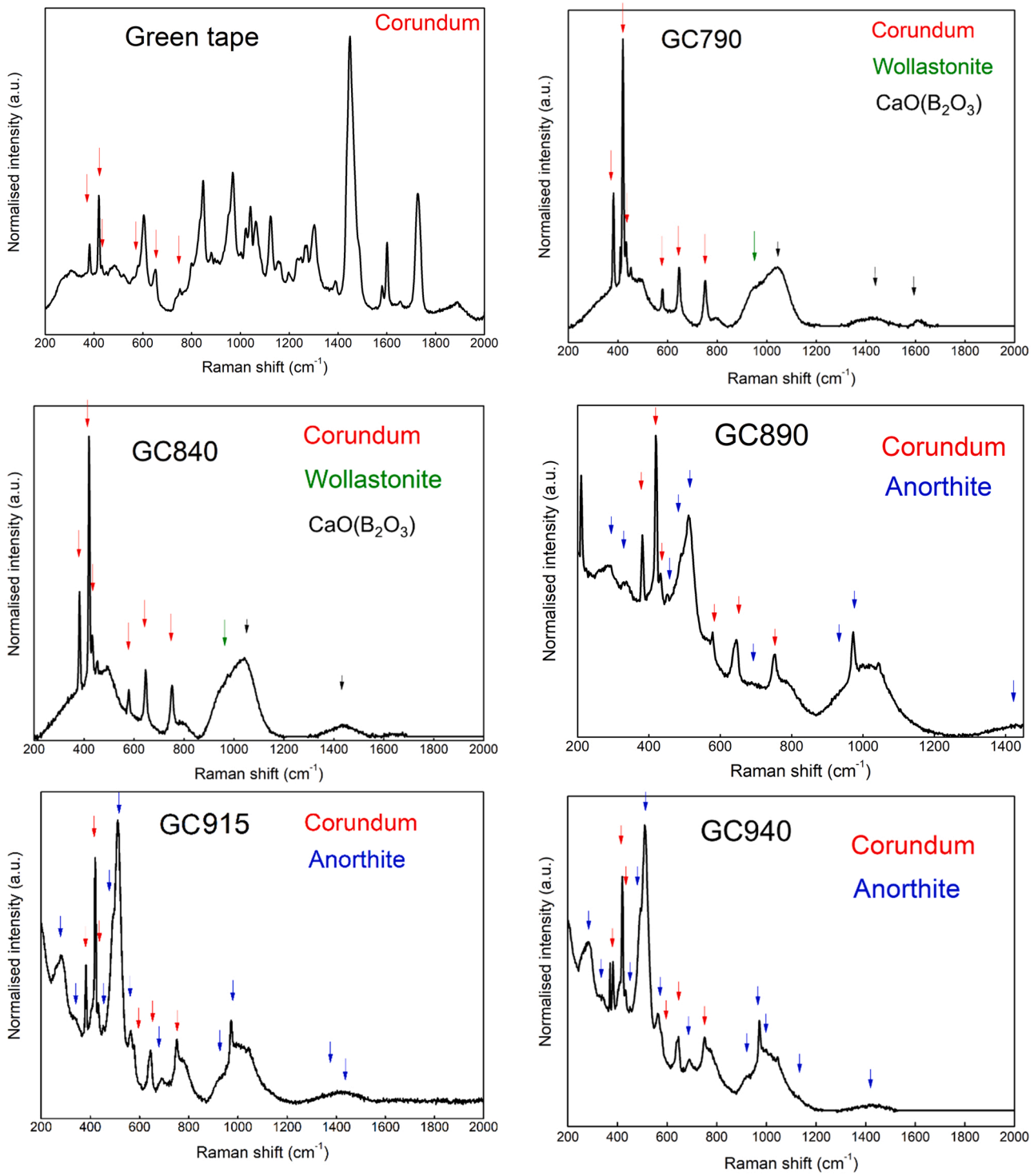

Fig. 8.. Normalized Raman spectra of the different GC samples. The maxima of the sample peaks were attributed to the reference peaks from RRUFF database. Blue arrows - anorthite, red arrows - corundum, black arrows - CaO (B_2O_3) matrix, green arrows - wollastonite.

results are in a good agreement with those gained from the XRD investigations.

In the next step, the *as-fired* samples were porosified in a 3 $molL^{-1}$ KOH solution for 2 h at 75 °C. The SEM micrographs of the porosified LTCC samples are shown in Fig. 13. As can be seen, the surface of the GC840 sample is strongly corroded after etching treatment. However, by increasing the firing peak temperature of the *as-fired* LTCC, after etching treatment, the resulting surface becomes smoother, and the etching is more controllable.

Given the etch parameters above, the penetration depth of the etching solutions decreases with increasing firing temperature from about 5 μm for GC840 to less than 0.5 μm for GC940. Furthermore, the weight loss percentage was quite low (less than 1 %) for all samples and even decreased when the peak firing temperature was increased. This could be attributed to the increased degree of densification due to the penetration of the melted glass into the free volumes between the grains for the LTCC samples fired at higher peak temperatures which in turn makes the LTCC more etch resistant. These results show that while a

Table 2
The relative atomic concentration of chemical elements on the surface of the samples, calculated from high resolution XPS spectra.

	Relative atomic concentration, at%					
	O	C	Ca	Al	Si	B
GC-green tape	24.5	67.6	1	3.2	2.8	0.9
GC790	52.5	14.7	4.7	11.5	13.1	3.5
GC840	53.5	14.6	4.6	8.6	15.8	2.9
GC890	54	15.7	5.4	6.4	16.7	1.8
GC915	56	14.2	4.6	4.2	18.6	2.4
GC940	56.4	13.4	4	4.2	19.4	2.6

Table 3
Chemical bond concentration calculated from deconvoluted Al 2p peaks of the samples.

	α-Al_2O_3, %	transition-Al_2O_3, %	Al-OH, %
GC-green tape	73	21	6
GC790	67	31	2
GC840	75	24	1
GC890	66	30	4
GC915	59	39	2
GC940	33	61	6

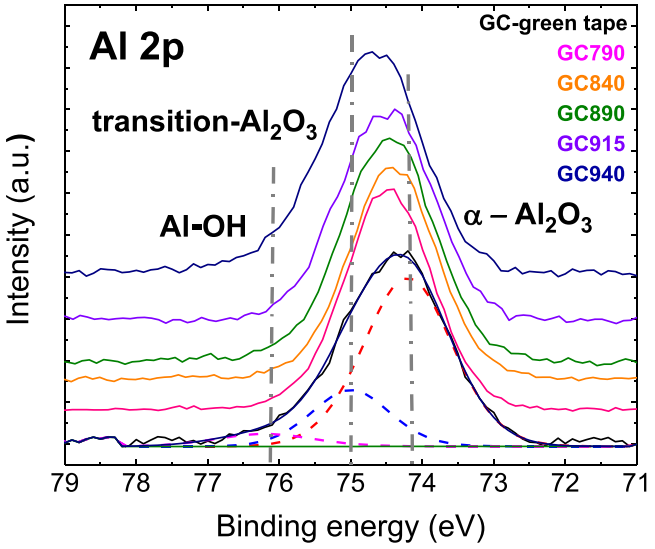

Fig. 9. Comparison of calibrated high-resolution Al 2p peaks of GC-green tapes fired at different peak temperatures. The shapes of Si 2p peaks are labeled as straight lines, the fitted components are labeled as dotted lines.

Table 4.
Chemical bond concentration, calculated from deconvoluted Si 2p peaks of the samples.

	SiC, %	SiO_2/Si,%	SiO_2, %
GC-green tape	5	70	25
GC 790	1	64	35
GC 840	1	57	42
GC 890	1	64	35
GC 915	1	53	46
GC 940	0.5	35	64.5

higher peak temperature is favorable for the fabrication of very smooth surfaces for the LTCC substrates in the *as-fired* state (see Fig. 3), it is not advantageous when a high degree of porosity is targeted.

Additionally, the etched samples were investigated with TEM (see Fig. 14). The pores for the GC940 appear to be the largest which could be

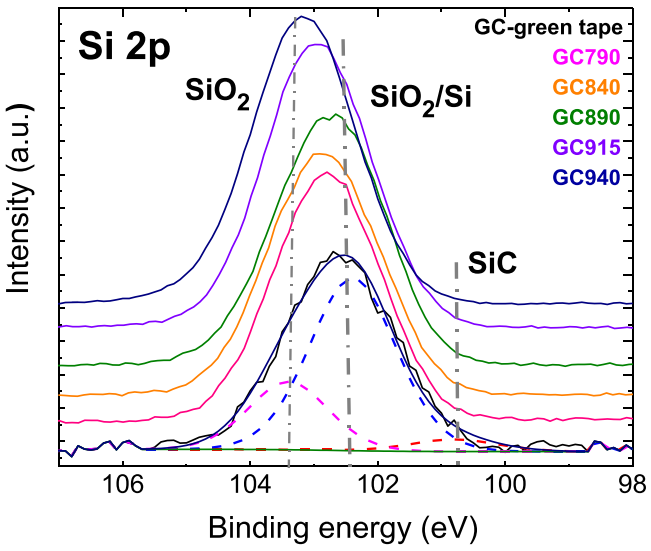

Fig. 10.. Comparison of calibrated high-resolution Si 2p peaks of GC-green tapes fired at different peak temperatures. The shapes of Si 2p peaks are labeled as straight lines, the fitted components are labeled as dotted lines.

Table 5.
Chemical bond concentration, calculated from deconvoluted O 1 s peaks of the samples.

	O bulk, %	Al-OH/CaCO, %	B_2O_3/SiO_2/H_2O, %
GC-green tape	16	43	41
GC790	35	51	14
GC840	31	49	20
GC890	22	55	23
GC915	17	52	31
GC940	12	66	22

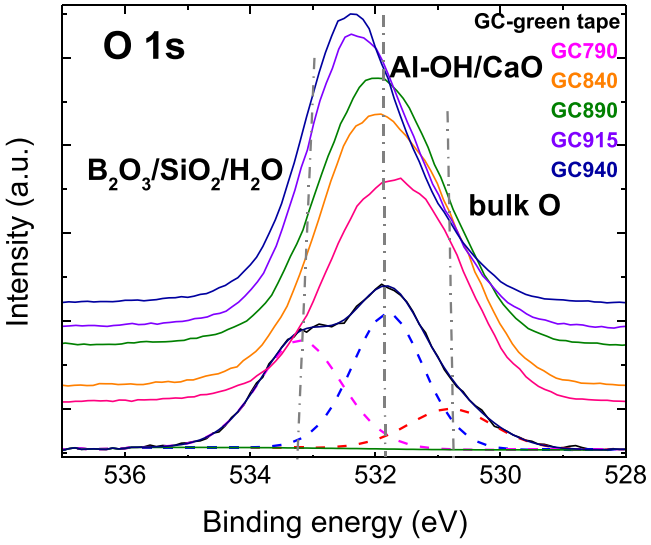

Fig. 11.. Comparison of calibrated high-resolution O 1s peaks of GC-green tapes fired at different peak temperatures. The shapes of Si 2p peaks are labeled as straight lines, the fitted components are labeled as dotted lines.

due to the highest amount of anorthite phase which is expected to be crystallized for this sample compared to others fired at lower temperatures. For the samples fired at lower temperatures, *i.e.* GC840 and GC890 where the *as-fired* sample was not well densified (see Fig. 3), the obtained prosity is not exclusively due to the etching process, but also due

Table 6.
The relative atomic concentration of chemical elements obtained by EDX.

	Relative atomic concentration, at%			
	O	Ca	Al	Si
GC790	65.4	5.4	18.9	10.3
GC840	65.7	4.8	18.8	10.7
GC890	69.1	5.3	14.3	11.3
GC915	69.5	3.8	14.4	12.3
GC940	69.4	3.4	13.9	13.3

to the inherent porosity of the substrate in the *as-fired* state.

Similar to the etching treatment of GC LTCC fired by an industry compatible process studied in our previous work [20], highly porous silica structures were observed in all samples after the etching treatment. These structures are generated from the laminar needle-like structures of thermodynamically unstable grown plagioclase feldspars which are typically found in the GC LTCC in the *as-fired* state. They are known to form at temperatures above 1100 K due to the Al and Si ordering in anorthite. Salje et al. have studied the formation of these needle-like structures in detail [49]. The formation of needle-like twin structures in the *as-fired* state of GC LTCC was also observed in the TEM investigations of Steinhäußer et al. [35]. They referred to these structures which are surrounding the alumina grains and are consisted of Si, Al, Ca, and O, as anorthic. However, no TEM investigations were carried out in their study on the etched samples. Nevertheless, the highly porous structures observed in Fig. 14, consist only of Si and O, which means that they are formed by the depletion of Ca and Al from the anorthite phase due to the etching treatment.

4. Conclusions

CeramTape GC which was chosen as a model system for state-of-the-art glass-ceramic LTCCs, is composed of alumina particles and glass and was selected for investigating the sintering behavior. By performing *in-situ* XRD measurements of GC LTCC green sheets up to temperatures around 825 °C, the corundum filler was found as the only crystalline phase. Above, the formation of wollastonite was detected. When the temperature is further increased above 875 °C, anorthite phase crystallizes from the glass phase matrix. Anorthite crystals preferentially grow near corundum grains, suggesting that corundum grains serve as active nucleation sites for anorthite.

A further temperature increase up to 925 °C leads to the formation of

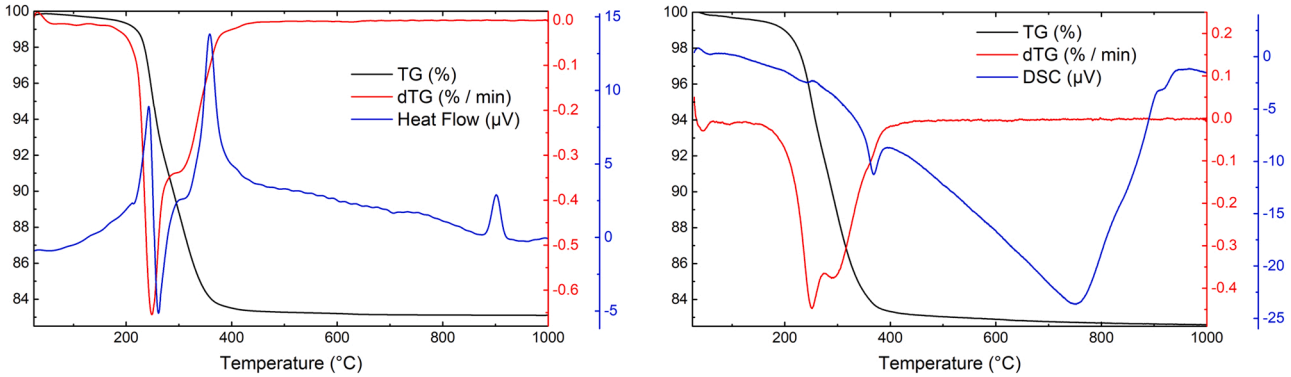

Fig. 12. Thermal analysis of CeramTape GC green tape. Left: TG-DTA; right: TG-DSC (heating rate 3 K/min).

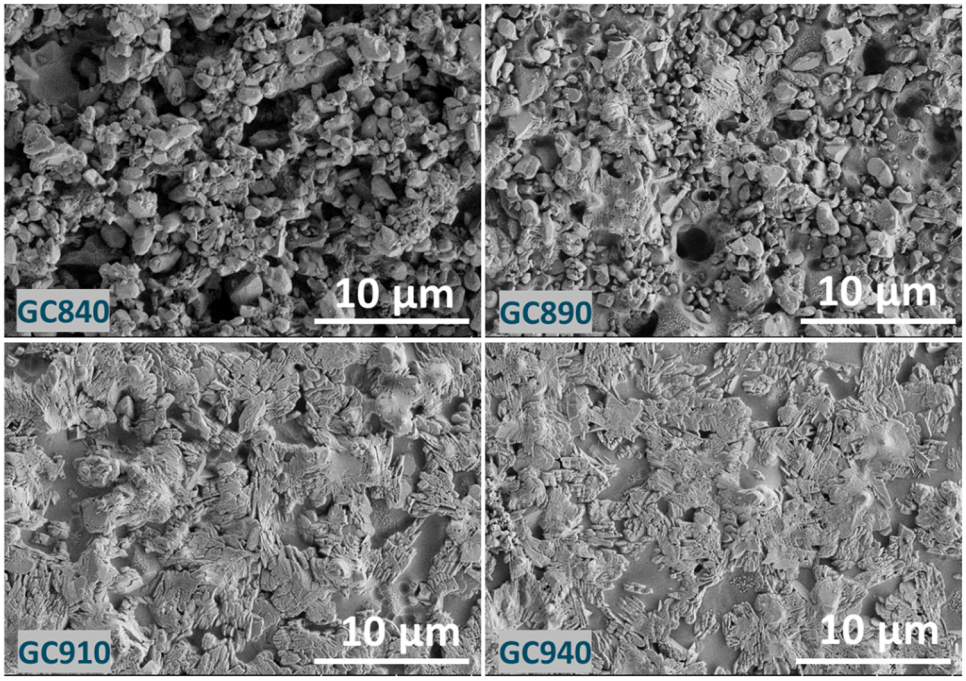

Fig. 13.. SEM images of the different *as-fired* GC LTCC substrates, etched for 2 h in 3 molL^{-1} KOH solution at 75 °C.

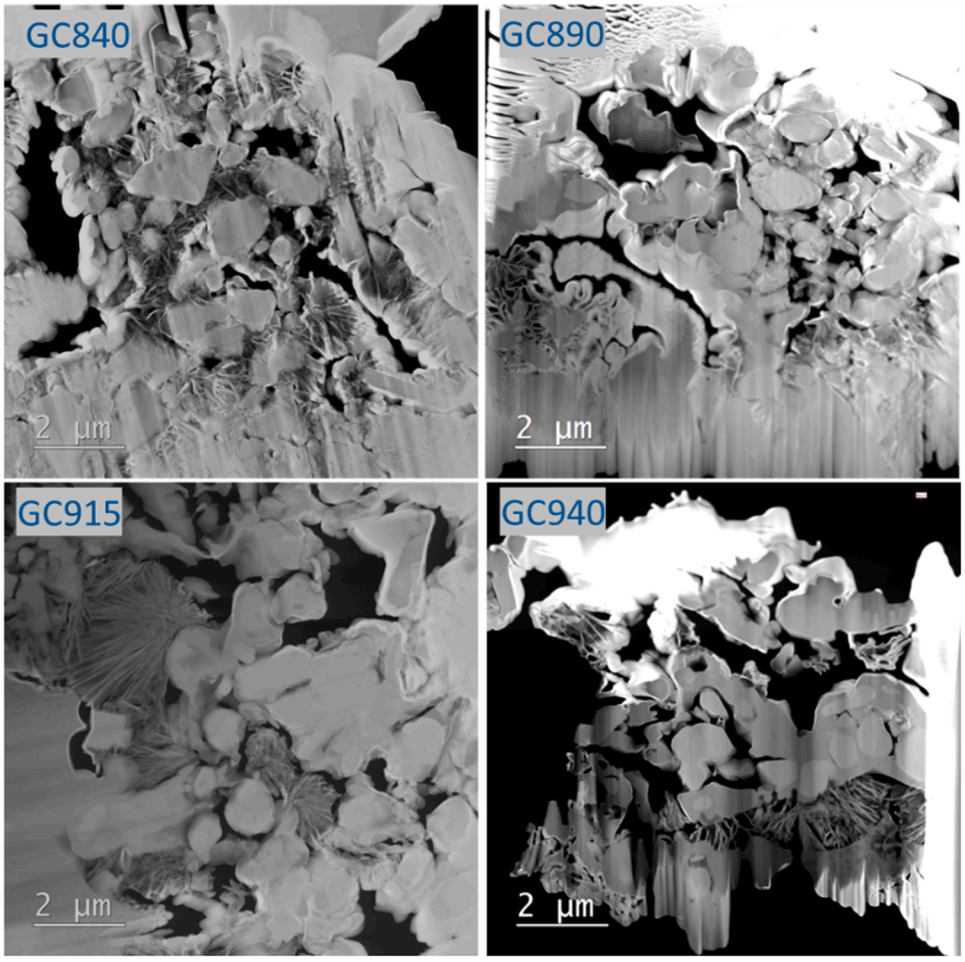

Fig. 14.. Overview of GC LTCC substrates etched in 3 mol L^{-1} KOH solution at 90 °C for 6 h for the substrates fired at different peak temperatures.

an additional anorthite phase while simultaneously the wollastonite fraction decreases. Beyond 925 °C, no perceptible change in the diffractograms is observed, except for the slight increase in the intensity of the newly formed anorthite peaks together with the decrease in the intensity of the corundum peaks. Furthermore, the wollastonite almost disappears above 950 °C. Therefore, it can be concluded that the anorthite crystallizes from the Al_2O_3-enriched glass around the corundum grains up to 925 °C. By a further increase of temperature to above 950 °C, the second step of anorthite crystallization occurs, where it grows at the expense of corundum and wollastonite.

The replacement of corundum with anorthite was further confirmed due to a correlative analysis of sintered glass-ceramics by Raman and XPS analyses. Moreover, it was found that by increasing the sintering temperature the glass diffuses close to the top layer of the samples which results in a smoother surface with lower open porosity which could be useful for fineline printing of LTCC.

A high-quality surface is critical for high-frequency applications because as frequency increases in the GHz range, the skin depth derived for ideally smooth conductor surfaces decreases in the order of surface roughness, resulting in a nearly linear increase in conduction losses.

Finally, etching investigations revealed non-selective removal of LTCC components, *i.e.,* the glass matrix and crystalline phases in an aqueous KOH solution. In addition, the formation of needle-like SiO_2 structures near the corundum grains were observed after the etching treatment, which was due to the depletion of Al and Ca from the anorthite phase. All in all, the present study provides useful information not only for the dimensional control and mechanical properties of the sintered tape, but also for the specific surface properties, chemical composition, and porosification behavior of conventional LTCC substrates, thus enabling further optimization of glass-ceramic material properties.

Declaration of Competing Interest

The authors declare that they have no known competing financial interests or personal relationships that could have appeared to influence the work reported in this paper.

Acknowledgements

The authors would like to acknowledge the financial support from the Austrian Science Fund (FWF), No. I 2551-N30. This work has also used research infrastructure CzechNanolab supported by the Ministry of Education, Youth and Sports of the Czech Republic through the LM2018110 project.

References

[1] A. Vasudev, A. Kaushik, K. Jones, S. Bhansali, Prospects of low temperature co-fired ceramic (LTCC) based microfluidic systems for point-of-care biosensing and environmental sensing, Microfluid. Nanofluidics 14 (3–4) (2013) 683–702.
[2] W. Zhang, R.E. Eitel, Biostability of low-temperature co-fired ceramic materials for microfluidic and biomedical devices, Int. J. Appl. Ceram. Technol. 9 (1) (2012) 60–66.
[3] N.C. Pesquero, M.R. Gongora-Rubio, H. Yamanaka, A novel LTCC electrochemical cell construction and characterization: a detection compartment for portable devices, Analyst 138 (15) (2013) 4298–4304.
[4] Y. Liang, M. Ma, F. Zhang, F. Liu, T. Lu, Z. Liu, Y. Li, Wireless microfluidic sensor for metal ion detection in water, ACS Omega 6 (13) (2021) 9302–9309.

[5] C. Galvis, T. Vaupel, T. Bertuch, M. Wilhelm, T. Wichmann, S. Tejero Alfageme, Feasibility of an automotive radar antenna at 77 GHz on LTCC substrate, IET Radar Sonar Navig. 12 (10) (2018) 1172–1178.

[6] H. Jantunen, T. Kangasvieri, J. Vähäkangas, S. Leppävuori, Design aspects of microwave components with LTCC technique, J. Eur. Ceram. Soc. 23 (14) (2003) 2541–2548.

[7] A.-C. Bunea, D. Neculoiu, M. Lahti, T. Vähä-Heikkilä, Ltcc microstrip parasitic patch antenna for 77 ghz automotive applications, in: Proceedings of the IEEE International Conference on Microwaves, Communications, Antennas and Electronic Systems (COMCAS 2013), IEEE, 2013, 1–4.

[8] Y.-S. Lin, C.-C. Liu, K.-M. Li, C.H. Chen, Design of an LTCC tri-band transceiver module for GPRS mobile applications, IEEE Trans. Microw. Theory Tech. 52 (12) (2004) 2718–2724.

[9] H. Tie, Z. Song, Q. Ma, L. Qian, S. Hu, B. Zhou, Dual-mode LTCC Filter with 2nd-order Harmonic Suppression for 5G Applications, in: Proceedings of the International Conference on Microwave and Millimeter Wave Technology (ICMMT), IEEE, 2021, 1–3.

[10] A. Bittner, H. Seidel, U. Schmid, High-frequency characterization of porous low-temperature cofired ceramics substrates, J. Am. Ceram. Soc. 93 (11) (2010) 3778–3781.

[11] M. Fischer, S. Gropp, J. Stegner, A. Frank, M. Hoffmann, J. Mueller, Silicon-ceramic composite substrate: a promising RF platform for heterogeneous integration, IEEE Microw. Mag. 20 (10) (2019) 28–43.

[12] H. Yu, J. Liu, W. Zhang, S. Zhang, Ultra-low sintering temperature ceramics for LTCC applications: a review, J. Mater. Sci.: Mater. Electron. 26 (12) (2015) 9414–9423.

[13] S. Kemethmüller, M. Hagymasi, A. Stiegelschmitt, A. Roosen, Viscous flow as the driving force for the densification of low-temperature co-fired ceramics, J. Am. Ceram. Soc. 90 (1) (2007) 64–70.

[14] C. Bienert, A. Roosen, Characterization and improvement of LTCC composite materials for application at elevated temperatures, J. Eur. Ceram. Soc. 30 (2) (2010) 369–374.

[15] A. Hajian, S. Smetaczek, C. Zellner, M. Stöger-Pollach, T. Konegger, A. Limbeck, U. Schmid, Tailored and deep porosification of LTCC substrates with phosphoric acid, J. Eur. Ceram. Soc. 39 (10) (2019) 3112–3119.

[16] K. Makarovič, A. Meden, M. Hrovat, J. Holc, A. Benčan, A. Dakskobler, M. Kosec, The effect of processing conditions on the properties of LTCC material, J. Am. Ceram. Soc. 95 (2) (2012) 760–767.

[17] T. Rabe, W.A. Schiller, T. Hochheimer, C. Modes, A. Kipka, Zero shrinkage of LTCC by self-constrained sintering, Int. J. Appl. Ceram. Technol. 2 (5) (2005) 374–382.

[18] C.D. Kumar, T. Sowmya, E. Sunny, N. Raghu, N. Venkataramani, A.R. Kulkarni, Influence of nature of filler on densification of anorthite-based crystallizable glass+ ceramic system for low temperature cofired ceramics application, J. Am. Ceram. Soc. 92 (3) (2009) 595–600.

[19] S. Kemethmüller, A. Roosen, F. Goetz-Neunhoeffer, J. Neubauer, Quantitative analysis of crystalline and amorphous phases in glass–ceramic composites like LTCC by the Rietveld method, J. Am. Ceram. Soc. 89 (8) (2006) 2632–2637.

[20] A. Hajian, M. Stöger-Pollach, M. Schneider, D. Müftüoglu, F.K. Crunwell, U. Schmid, Porosification behaviour of LTCC substrates with potassium hydroxide, J. Eur. Ceram. Soc. 38 (5) (2018) 2369–2377.

[21] R.M. German, P. Suri, S.J. Park, Liquid phase sintering, J. Mater. Sci. 44 (1) (2009) 1–39.

[22] J. Luo, The Development and Biocompatibility of Low Temperature Co-Fired Ceramic (LTCC) for Microfluidic and Biosensor Applications, University of Kentucky, 2014.

[23] R. Müller, R. Meszaros, B. Peplinski, S. Reinsch, M. Eberstein, W.A. Schiller, J. Deubener, Dissolution of alumina, sintering, and crystallization in glass ceramic composites for LTCC, J. Am. Ceram. Soc. 92 (8) (2009) 1703–1708.

[24] M. Rauscher, A. Roosen, Influence of low-temperature co-fired ceramics green tape characteristics on shrinkage behavior, Int. J. Appl. Ceram. Technol. 4 (5) (2007) 387–397.

[25] A. Mohanram, G.L. Messing, D.J. Green, Densification and sintering viscosity of low-temperature co-fired ceramics, J. Am. Ceram. Soc. 88 (10) (2005) 2681–2689.

[26] A. Bittner, U. Schmid, The porosification of fired LTCC substrates by applying a wet chemical etching procedure, J. Eur. Ceram. Soc. 29 (1) (2009) 99–104.

[27] A. Hajian, D. Müftüoglu, T. Konegger, M. Schneider, U. Schmid, On the porosification of LTCC substrates with sodium hydroxide, Compos. Part B Eng. 157 (2019) 14–23.

[28] A. Hajian, M. Brehl, T. Koch, C. Zellner, S. Schwarz, T. Konegger, D. de Ligny, U. Schmid, Wet-chemical porosification of LTCC substrates: dissolution mechanism and mechanical properties, Microporous Mesoporous Mater. 288 (2019), 109593.

[29] A. Hajian, T. Konegger, K. Bielecki, B. Mieller, T. Rabe, S. Schwarz, C. Zellner, U. Schmid, Wet chemical porosification with phosphate buffer solutions for permittivity reduction of LTCC substrates, J. Alloy. Compd. 863 (2021), 158059.

[30] J.B. Ollagnier, O. Guillon, J. Rödel, Effect of anisotropic microstructure on the viscous properties of an LTCC material, J. Am. Ceram. Soc. 90 (12) (2007) 3846–3851.

[31] R.-J. Xie, R. Zuo, E. Aulbach, U. Mackens, N. Hirosaki, J. Rödel, Uniaxial viscosity of low-temperature cofired ceramic (LTCC) powder compacts determined by loading dilatometry, J. Eur. Ceram. Soc. 25 (4) (2005) 417–424.

[32] W. Smetana, B. Balluch, G. Stangl, S. Lüftl, S. Seidler, Processing procedures for the realization of fine structured channel arrays and bridging elements by LTCC-Technology, Microelectron. Reliab. 49 (6) (2009) 592–599.

[33] G. Berthomé, E. N'Dah, Y. Wouters, A. Galerie, Temperature dependence of metastable alumina formation during thermal oxidation of FeCrAl foils, Mater. Corros. 56 (6) (2005) 389–392.

[34] M. Franz, I. Atassi, A. Maric, B. Balluch, M. Weilguni, W. Smetana, C. Kluge, G. Radosavljevic, Material characteristics of the LTCC base material CeramTape GC, in: Proceedings of the Thirty Fifth International Spring Seminar on Electronics Technology, IEEE, 2012, 276–281.

[35] F. Steinhäußer, K. Hradil, S. Schwarz, W. Artner, M. Stöger-Pollach, A. Steiger-Thirsfeld, A. Bittner, U. Schmid, Wet chemical porosification of LTCC in phosphoric acid: anorthite forming tapes, J. Eur. Ceram. Soc. 35 (15) (2015) 4181–4188.

[36] M. Eberstein, T. Rabe, W.A. Schiller, Influences of the glass phase on densification, microstructure, and properties of low-temperature co-fired ceramics, Int. J. Appl. Ceram. Technol. 3 (6) (2006) 428–436.

[37] R.E. Benner, J. Mitchell, R. Grow, Raman scattering as a diagnostic technique for cathode characterization, IEEE Trans. Electron Devices 34 (8) (1987) 1842–1847.

[38] A.S. Jbara, Z. Othaman, M. Saeed, Structural, morphological and optical investigations of θ-Al_2O_3 ultrafine powder, J. Alloy. Compd. 718 (2017) 1–6.

[39] P. Richet, P. Gillet, A. Pierre, M.A. Bouhifd, I. Daniel, G. Fiquet, Raman spectroscopy, x-ray diffraction, and phase relationship determinations with a versatile heating cell for measurements up to 3600 K (or 2700 K in air), J. Appl. Phys. 74 (9) (1993) 5451–5456.

[40] V. Simon, M. Todea, A. Takács, M. Neumann, S. Simon, XPS study on silica–bismuthate glasses and glass ceramics, Solid State Commun. 141 (1) (2007) 42–47.

[41] Y. Tanizawa, T. Suzuki, Effects of silicate ions on the formation and transformation of calcium phosphates in neutral aqueous solutions, J. Chem. Soc., Faraday Trans. 91 (19) (1995) 3499–3503.

[42] J.T. Kloprogge, L.V. Duong, B.J. Wood, R.L. Frost, XPS study of the major minerals in bauxite: gibbsite, bayerite and (pseudo-) boehmite, J. Colloid Interface Sci. 296 (2) (2006) 572–576.

[43] E. Korin, N. Froumin, S. Cohen, Surface analysis of nanocomplexes by X-ray photoelectron spectroscopy (XPS), ACS Biomater. Sci. Eng. 3 (6) (2017) 882–889.

[44] D.J. Joyner, D.M. Hercules, Chemical bonding and electronic structure of B_2O_3, H_3BO_3, and BN: An ESCA, Auger, SIMS, and SXS study, J. Chem. Phys. 72 (2) (1980) 1095–1108.

[45] A.V. Naumkin, A. Kraut-Vass, S.W. Gaarenstroom, C.J. Powell, NIST standard reference database 20, version 4.1, Natl. Inst. Stand. Technol. NIST (2012) 1–49.

[46] A. Burke, C. Brown, W. Bowling, J. Glaub, D. Kapsch, C. Love, R. Whitaker, W. Moddeman, Ignition mechanism of the titanium–boron pyrotechnic mixture, Surf. Interface Anal. 11 (6–7) (1988) 353–358.

[47] A.K. Rumaiz, C. Jaye, J. Woicik, W. Wang, D. Fischer, J. Jordan-Sweet, C. Chien, Boron migration due to annealing in CoFeB/MgO/CoFeB interfaces: a combined hard x-ray photoelectron spectroscopy and x-ray absorption studies, Appl. Phys. Lett. 99 (22) (2011), 222502.

[48] C. Zhou, Y. Tang, W. Wang, S. Zhou, L. Zhao, H. Li, H. Diao, Preparation of p^+-layers using water vapour as oxidant in BBr_3 diffusion for silicon solar cells, J. Phys. D Appl. Phys. 46 (28) (2013), 285102.

[49] E.K. Salje, A. Buckley, G. Van Tendeloo, Y. Ishibashi, G.L. Nord, Needle twins and right-angled twins in minerals; comparison between experiment and theory, Am. Mineral. 83 (7–8) (1998) 811–822.